Research Signpost
37/661 (2), Fort P.O., Trivandrum-695 023, Kerala, India

Phase Transitions. Applications to Liquid Crystals, Organic Electronic and Optoelectronic Fields, 2006: 97-113 ISBN: 81-308-0062-4 Editor: Vlad Popa-Nita

5 Influence of finite size, randomness and wetting on confined liquid crystal phases

Zdravko Kutnjak[2], Samo Kralj[1,2] and Gojmir Lahajnar[2]
[1]Laboratory of Physics of Complex Systems, Faculty of Education, University of Maribor, Koroška 160, 2000 Maribor, Slovenia; [2]Jožef Stefan Institute Jamova 39, 1000 Ljubljana, Slovenia

Abstract

A calorimetric study of the temperature driven phase behavior of octylcyanobiphenyl (8CB) liquid crystal confined to a controlled-pore glass (CPG) is presented. The CPG matrices characterized with void radia ranging from 10 nm to 200 nm were used. The CPG voids were either left non-treated or were treated with silane. We focus on the influence of R and surface treatment on the isotropic-nematic (I-N) and nematic-smectic A (N-SmA) phase transition as the temperature is varied. We find out that the surface wetting dominates the I-N and N-SmA phase transition temperatures. The specific heat critical behavior at the

Correspondence/Reprint request: Dr. Samo Kralj, Laboratory of Physics of Complex Systems, Faculty of Education, University of Maribor, Koroška 160, 2000 Maribor, Slovenia. E-mail: samo.kralj@uni-mb.si

N-SmA transition further reveals presence of finite size effects and randomness introduced by CPG confinement.

5.1. Introduction

In recent years there have been many studies devoted to the study of phase behavior of various liquid crystal (LC) phases confined to different porous matrices [1]. Such systems are typical representatives of complex systems displaying an extremely rich palette of behaviors. This richness mostly arises due to the softness [2] of LC phases, i.e., their strong response to a relatively weak disturbance. Among the different phenomena the influence of finite size effects, wetting, randomness and combination thereof is of particular interest.

As confining matrices one commonly uses controlled-pore glasses (CPGs) [3, 4], Vycor glasses [5], Russian glasses [6] and aerogels [7]. The inherent randomness imposed by geometry is largest in aerogels and lowest in CPGs. These systems are characterized by an average characteristic void size ranging between μm and nm. The controlled-pore glass consists of a strongly connected network of curved cylindrically shaped pores with a relatively narrow distribution of cross-sectional radii. The Vycor glass has similar geometrical characteristics with the exception that local deviations from the cylindrical geometry are larger. In the case of Russian glasses and aerogels the voids are of rather irregular shape and even more strongly interconnected.

Different experimental techniques (precision calorimetry [8], x-rays [9], light scattering [10], deuterium NMR [11], dielectric spectroscopy [12], Kerr effect [13]) have led essentially to the same conclusion that the behavior of LCs immersed in porous matrices strongly depend on the mean characteristic pores' void size R, the interconnectedness of voids, as well as the anchoring and wetting properties of voids' surface. The following general characteristics have been observed. (i) Bulk transition temperatures T_c of the isotropic-nematic or nematic-smectic phase could be shifted either upward [3] or in most cases downward [4] by several degrees. The direction and magnitude of the phase transition temperature shift ΔT_c strongly depends on R and on the ordering properties of the cavity surface. (ii) With decreasing value of R the phase transition regime progressively broadens for $R > R_c$. Below the critical void size R_c, which is comparable to the relevant order parameter correlation length, the phase transition is replaced by a gradual evolution of the order parameter. (iii) In many cases the surface induced prewetting phenomena are observed in case of strong surface interactions. (iv) In all matrices finite size effects are observed. In addition to these phenomena one also expects that a domain type pattern is realized in these samples [14]. Well defined domains appear if (i) a continuous symmetry is broken at the phase transition and (ii) for a relatively weak influence of confining surfaces introducing into the

system a quenched disorder. Note that the existence of the domain pattern is still debatable [15].

In this contribution we study the phase behavior of octylcyanobiphenyl (8CB) liquid crystal confined to a controlled-pore glass. The CPG voids were either non-treated or treated with silane. The temperature behavior across the isotropic-nematic (*I-N*) and nematic-smectic A (*N-SmA*) phase transition is measured with the high precision calorimetry. We analyze the role of surface wetting properties, randomness and finite size effects. Some of observed phenomena can be well reproduced using a bicomponent single pore type phenomenological model.

The outline of the paper is as follows. In Sec. II we present the experimental set up. In. Sec. III the theoretical background is given. The phase behavior is analyzed in Sec. IV. The conclusions are summarized in Sec. V.

5.2. Experimental set up

5.2.1. Sample

The molecules of the liquid crystal octylcyanobiphenyl (8CB) consist of two phenyl rings and the octyl tail. In bulk the 8CB exhibits a weakly 1^{st} order *I-N* and the 2^{nd} order *N-SmA* phase transition. The latent heat of the *I-N* phase transition, taking place at $T_{IN} \sim 314$ K, is roughly $L \sim 2.2$ J/g. The *SmA* phase is established below $T_{NA} \sim 307$ K where the LC molecules are organized in bilayers. Note that the exact nature of the *N-SmA* transition is still debatable. Some authors claim this transition is very weakly 1^{st} order [16].

As a confining medium we use the controlled-pore glass. The scanning electron micrograph (SEM) of a typical empty CPG matrix is shown in Fig. 5.1.

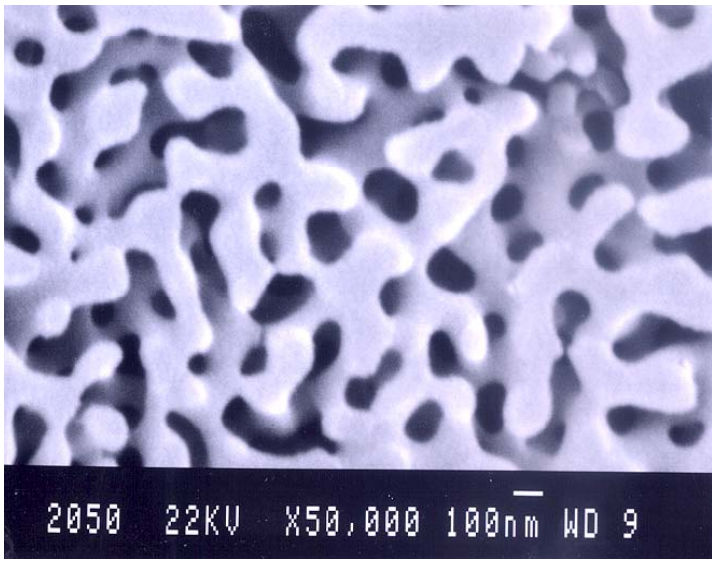

Figure 5.1. The SEM photograph of an empty controlled-pore glass matrix with $2R$ = 127.3 nm.

The CPG voids resemble curved and strongly interconnected cylinders of radii R. We use CPG matrices of the mean pore diameter ranging from 23.7 to 395 nm with a standard deviation of 5 – 10%. The void surface of the CPG is smooth down to the nm scale, with no preferred direction within the surface plane. The CPG voids were either treated with silane or left non-treated. We henceforth refer to these samples as *silane-treated* and *non-treated*, respectively. The non-treated CPG void surfaces enforce the isotropic tangential orientational anchoring to the LC molecules. Because of steric effects the orientation along the void's long axis is chosen as the easy axis among the degenerate set of easy axes. In silane-treated CPG samples the pore surface enforces homeotropic orientational anchoring to the LC molecules.

The CPG matrices were filled with 8CB in the isotropic phase. Prior to filling, the CPG matrices were cleaned by immersing them into a 1 : 1 mixture of concentrated H_2SO_4 and HNO_3 for 24 h. Afterwards they were extensively washed in distilled deionized water and evacuated. This procedure was repeated until a neutral pH of water containing CPG particles was established. Then the CPG matrices were dried in vacuum at 250 °C for 24 h.

Silane-treated CPG matrices were prepared by immersing the cleaned CPG matrices for 10 min in a 2% water solution of octadecyldimethyl (3-trimethoxysilypropyl) ammonium chloride ($C_{26}H_{58}ClNO_3Si$). The matrices were then dried in vacuum at 110 °C for 48 h.

5.2.2 Calorimetric measurements

Heat-capacity data were acquired by a computerized calorimeter, which is capable of automated operation in either ac or relaxation modes. Description of the technique was extensively given in Ref.[17, 4]. The sample was contained in a sealed silver cell of approximately 0.5 mm thickness and 10 mm diameter. The sample cell is thermally linked to a temperature-stabilized bath (within ±0.1 mK) by support wires and by air. The thermal link can be represented in the temperature range of interest by a thermal resistivity $R_T \sim 270$.

In the *ac mode*, an oscillating heat $P_{ac}e^{i\omega t}$ with the frequency $\omega = 0.0767s^{-1}$ chosen so that $\omega << 1/\tau_{int}$ is supplied to the sample by a thin resistive heater. Here τ_{int} is the characteristic time for thermal diffusion in the sample cell. The temperature oscillations $T_{ac} = P_{ac}/(1/R_T + i\omega C)$ of the sample are detected by a small bead 1 MΩ thermistor. The complex heat capacity $C = C'(\omega) - iC''(\omega)$ could be in most cases considered as a real frequency-independent quantity $C = C'(0)$. Because the ac mode is less sensitive to the effects associated with the latent heat it does not provide a quantitative value of the latent heat in the case of the first-order phase conversion. However, an anomalous response in the phase shift $\Phi = \arctan(1/\omega R_T C' + C'/C'')$ of T_{ac} is typically observed [17] within the coexistence range of the first-order phase transition. So the phase

shift Φ can be useful in discriminating between the first- and second-order phase transition.

The ac heat capacity data were taken on cooling the sample from isotropic phase with the cooling rate between 100 – 300 mK/h. Near the phase transitions the cooling rate was typically reduced to 50 – 100 mK/h. The amplitudes of T_{ac} were between 5 mK and 20 mK with typical values near phase transitions between 5 – 10 mK. The mass of the samples was between 35 – 45 mg. The heat capacities of the empty silver cell (including the heater, thermistor, and support wires) were later subtracted from the C_p data in order to obtain the net heat capacity C_p of the sample. This net heat capacity of the sample was later divided by the mass of the sample in order to obtain the specific heat capacity C_p in J/gK. By subtracting further the nearly linear noncritical phonon background contribution the excess heat capacity ΔC_p related to the change of enthalpy at particular transition was obtained.

The *relaxation-mode* data have slightly lower signal to noise ratio than ac data and are therefore less suitable for analysis of the critical behavior in the case of second order phase transitions. However, the advantage of this mode, known also as nonadiabatic scanning mode, is much better sensitivity to latent heat than the ac mode, thus allowing the quantitative estimation of the discontinuous jump in the enthalpy H due to the first-order phase conversion. In the relaxation mode, the bath temperature is first stabilized, then the linearly ramped heater power is supplied to the cell [17]. During the heating run, $P = 0$ for $t < 0$, $P = \dot{P}t$ for $0 \le t \le t_1$, and $P = \dot{P}t_1 = P_0$ for $t > t_1$. For $t \le t_1$ the initial sample temperature is equal to the bath temperature T_B. For $t >> t_1$ the sample temperature reaches a plateau $T(\infty) = T_B + R_T P_0$. In the case of a cooling run the heater power profile is reversed: $P = P_0$ for $t < 0$, $P = P_0 - \dot{P}t$ for $0 \le t \le t_1$, and $P = 0$ for $t > t_1$. The initial and final sample temperatures are $T(\infty)$ and T_B, respectively. Here typically $t_1 \approx 480$ s during which 1540 sample temperature $T(t)$ data points were taken. In our case, the typical ramping steps $T(\infty) - T_B$ used were between 0.8 – 1.2 K. By applying the sample cell temperature variation analysis (described in detail in [17]) the effective heat capacity is then calculated from

$$C_{eff}(T) = \frac{dH}{dT} = \frac{P - (T - T_B)/R_T}{dT/dt}, \tag{5.1}$$

where $R_T = [T(\infty) - T_B]/P_0$ and P is the power at some time $0 \le t \le t_1$ corresponding to the sample temperature T between T_B and $T(\infty)$. Sample temperature heating/cooling rate dT/dt is calculated over a short time interval centered at t. Except for $t > t_1$ and a brief period of time just after $t = 0$ the temperature rate dT/dt is nearly linear. The total enthalpy H is calculated as

$H = \int C_{eff} dT$. By subtracting from C_{eff} the nearly linear non-critical phonon background contribution the excess enthalpy $\Delta H = \delta H + L$ could be obtained. Here δH represents continuous contribution to the total excess enthalpy and L denotes the discontinuous latent heat contribution.

Temperature dependence of C_p data obtained in an ac mode for different CPG samples are shown in Figs. 5.2 and 5.3.

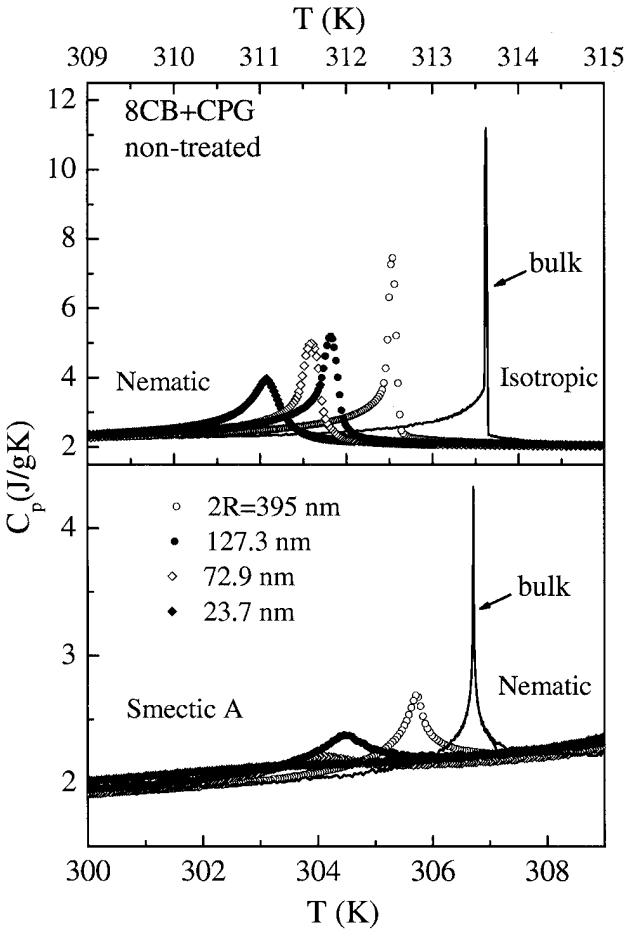

Figure 5.2. Temperature dependence of C_p data obtained in an ac mode for different CPG non-treated samples. The bulk 8CB reference sample is also added. The *I-N* and *N-SmA* transitions are shown in the upper and bottom part of the figure, respectively.

5.3 Model

5.3.1 Free energy

In order to explain the experimental results we use the Landau-de Gennes phenomenological approach [18]. The tensor nematic order parameter $\underline{Q} = S(\vec{n} \otimes \vec{n} - \frac{1}{3}\underline{I})$ describes the orientational uniaxial degree of ordering. Here $\vec{n}$ is the nematic director field, S the uniaxial order parameter, $\otimes$ stands for the tensorial product and $\underline{I}$ is the unit tensor. In this description we neglect biaxial

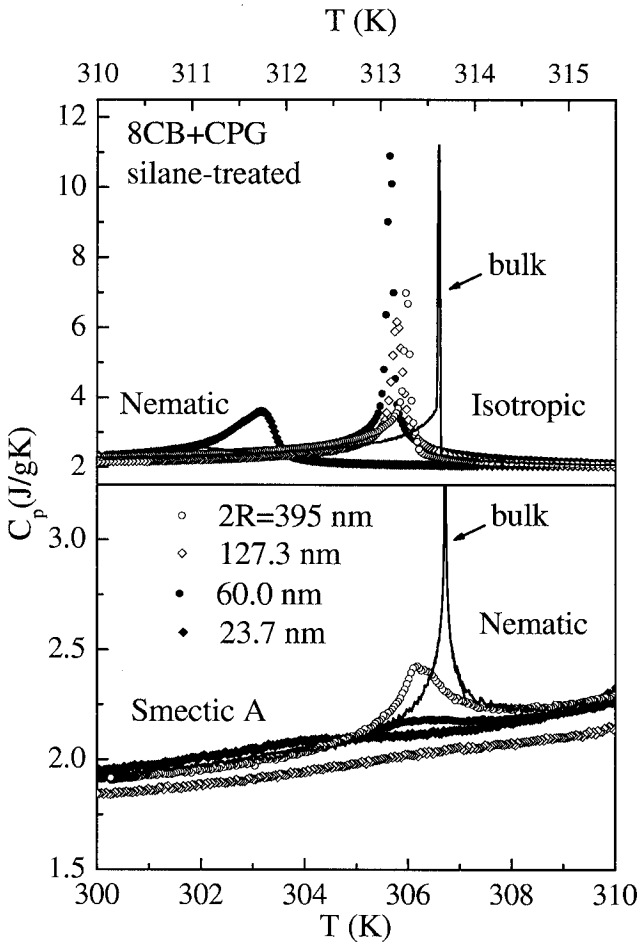

Figure 5.3. Temperature dependence of C_p data obtained in an ac mode for different CPG silan-treated samples. The bulk 8CB reference sample is also added. The *I-N* and *N-SmA* transitions are shown in the upper and bottom part of the figure, respectively.

effects. The smectic layer ordering is approximated with the complex order parameter $\psi = \eta e^{i\phi}$. The translational order parameter η describes the degree of smectic ordering and the phase factor ϕ defines the position of smectic layers. For more details concerning the order parameter fields we refer the reader to Ref.[19].

In terms of these fields we express the free energy

$$F = \int (f_c^{(n)} + f_c^{(s)} + f_e^{(n)} + f_e^{(s)} + f_{cp}) d^3\mathbf{r} + \int \left(f_i^{(n)} + f_i^{(s)} \right) d^2\mathbf{r} \tag{5.2}$$

of the confined liquid crystal phase, focusing on the *N-SmA* phase transition. The first integral in Eq. (5.2) describes the LC volume and the second one the LC-CPG interface contribution. The superscript $^{(phase)}$ refers either to the nematic (*phase* = *n*) or smectic (*phase* = *s*) contribution. The subscript $_j$ stands for the condensation (*j* = *c*), elastic (*j* = *e*), coupling (*j* = *cp*), or (*j* = *i*) interface contribution. In the lowest approximation we express the volume terms as

$$f_c^{(n)} \sim \frac{3a_0(T-T_*)}{2} Tr\underline{Q}^2 - \frac{9b}{2} Tr\underline{Q}^3 + \frac{9c}{2} Tr\underline{Q}^4 \tag{5.3}$$

$$= a_0(T-T_*)S^2 - bS^3 + cS^4, \tag{5.4}$$

$$f_c^{(s)} \sim \alpha_0(T-T_{NA})\,|\psi|^2 + \frac{\beta}{2}\,|\psi|^4 \tag{5.5}$$

$$= \alpha_0(T-T_{NA})\eta^2 + \frac{\beta}{2}\eta^4, \tag{5.6}$$

$$f_{cp} \sim -DS\eta^2, \tag{5.7}$$

$$f_e^{(n)} \sim L\,|\nabla Q|^2 \sim L\,|\nabla S|^2 + LS^2\,|\nabla \vec{n}|^2, \tag{5.8}$$

$$f_e^{(s)} \sim C_\perp\,|(\vec{n}\times\nabla)\psi|^2 + C_\parallel\,|(\vec{n}\cdot\nabla - iq_0)\psi|^2. \tag{5.9}$$

The quantities a_0, T_*, b, c, α_0, β, T_{NA}, D are the material constants. They enter the system via $f_c^{(n)} + f_c^{(s)} + f_{cp}$ and determine the bulk equilibrium values of order parameters $S \equiv S_b(T)$ and $\eta \equiv \eta_b(T)$ for undistorted (i.e., $f_e^{(n)} = f_e^{(s)} = f_i^{(n)} = f_i^{(s)} = 0$) LC ordering. In the case of negligible coupling (i.e., $D = 0$) the 1st order *I-N* and the 2nd order *N-SmA* phase transition take place at $T \equiv T_{IN} = T_* + \frac{b^2}{4a_0c}$ and $T \equiv T_{NA}$, respectively. A strong enough coupling term f_{cp} can change the character of the *N-SmA* transition [7]. The elastic terms describe the elastic penalties for distortions in the nematic $\left(f_e^{(n)}\right)$ and smectic $\left(f_e^{(s)}\right)$ degrees. Here the undistorted structure refers to the homogeneously aligned configuration along $\vec{n}$. In it the smectic layers are stacked along $\vec{n}$ and separated for the distance $d_0 = 2\,\pi/q_0$. The elastic LC properties are described with the positive representative bare nematic (L), smectic bend ($C_\perp$) and smectic compressibility ($C_\parallel$) elastic constant. We henceforth set $C_\perp \sim C_\parallel \sim C$, neglecting the smectic elastic anisotropy.

The dominant interface free energy density contributions are expressed as [18, 20]

$$f_i^{(n)} = W^{(n)}\nu\cdot\mathbf{Q}\cdot\nu = W^{(n)}S\left((\mathbf{n}\cdot\nu)^2 - 1/3\right), \tag{5.10}$$

$$f_i^{(s)} = -\frac{W^*\psi + W\psi^*}{2} = -W^{(s)}\eta\cos(\phi-\varphi), \tag{5.11}$$

and $W = W^{(s)}e^{i\varphi}$. The quantities $W^{(phase)}$ stand for the characteristic orientational ($W^{(n)}$) and translational ($W^{(s)}$) anchoring constant, ν is the local normal of the LC-CPG interface and φ is the phase factor favored by the interface. For the i)

silane-treated and ii) non-treated sample we set i) $W^{(n)} = -W_{sil}^{(n)}$, $\varphi = \varphi_{sil} \equiv 0$ and ii) $W^{(n)} = W_{non}^{(n)}$, $\varphi = \varphi_{non} \equiv qz$. Here $W_{sam}^{(phase)} > 0$ and the subscript $_{sam}$ labels the non-treated (*sam* = *non*) or silane-treated (*sam* = *sil*) sample. With such parametrization we enforce for the silane-treated sample the homeotropic orientational anchoring and the growth of smectic layers from the interface towards the void interior. For the non-treated sample we enforce isotropic tangential orientational anchoring and the growth of layers with periodicity $q \sim q_0$ along the *z*-coordinate describing the direction along the void's long axis. Here we assumed that the periodicity q was imprinted and memorized on the interface by the SmA phase in contact with it [21, 22].

Note that we have introduced only the most essential free energy terms that are essential for qualitative explanation of measured results.

In addition to the radius R, introduced by the geometry of the system, the competition between the condensation, elastic and interface interactions introduce also material dependent characteristic lengths. The most important for our study are the nematic ($\xi^{(n)}$) and smectic ($\xi^{(s)}$) order parameter correlation lengths, the smectic penetration length λ, and the nematic $\left(d_e^{(n)}\right)$ and smectic $\left(d_e^{(s)}\right)$ surface extrapolation lengths.

They are roughly expressed as [18]

$$\xi^{(n)}(T) \sim \sqrt{\frac{L}{\frac{1}{2}\frac{\partial^2 f_c^{(n)}}{\partial S^2}}}, \xi^{(s)}(T) \sim \sqrt{\frac{C}{\frac{1}{2}\frac{\partial^2 f_c^{(s)}}{\partial \eta^2}}}, \tag{5.12}$$

$$\lambda \sim \sqrt{\frac{S_b^2 L}{\eta_b^2 C q_0^2}}, \tag{5.13}$$

$$d_e^{(n)} \sim \frac{L}{W_{sam}^{(n)}}, d_e^{(s)} \sim \frac{C}{W_{sam}^{(s)}}. \tag{5.14}$$

The second derivatives in expressions for ($\xi^{(n)}$) and ($\xi^{(s)}$) are expressed at equilibrium values $S = S_b(T)$ and $\eta = \eta_b(T)$, respectively.

A further length R_d can be introduced if a relatively weak disorder is present in the system, as described in detail in Ref.[19]. The necessary condition is that a continuous symmetry was broken at a relevant phase transition. In our case the continuous orientational and translational symmetries are broken at T_{IN} and T_{NA}, respectively. This loss of symmetry appears in the so called hydrodynamic fields, represented by $\vec{n}(\vec{r})$ in the nematic and by $\phi(\vec{r})$ in the SmA phase. The perturbations of hydrodynamic fields evolve on the geometrically available length in the system. The length R_d reveals the balance between the elastic and disorder tendencies. It introduces a

kind of domain structure in the system. In our samples the disorder is introduced geometrically via random inter-void connections and a relatively random void curvature. Note that there is still not a clear consensus about this length, although several experimental studies confirm this belief.

5.3.2 Effective scaled free energy density

We next derive the effective free energy of the sample. From it the phase behavior can be predicted on varying controlling parameters. We assume that the system exhibits a domain-like pattern in which the geometry of the CPG voids is imprinted. Consequently we predict that a typical domain resembles a cylindrical void of radius R and length R_d. The length R_d depends on the disorder strength and is the free parameter in the model. We further assume that at the LC-void interface, described by $\vec{r} = \vec{r}_i$, the degree of LC ordering strongly differs from that in the central region, described by the radius vector $\vec{r} = \vec{r}_V$. We set $S(\vec{r}_i) \sim S_i$, $\eta(\vec{r}_i) \sim \eta_i$, $S(\vec{r}_V) \sim S$, $\eta(\vec{r}_V) \sim \eta$). We refer to this approximation as the *two-component approach*.

We take into account that perturbations in the order parameter fields $S(\vec{r})$ and $\eta(\vec{r})$ in a bulk-like environment evolve over the scale given by the relevant order parameter correlation length. In confined systems finite size effects must be taken into account if a correlation length becomes comparable to a characteristic geometrically imposed length R_g. In case of CPG samples this can be either $2R$ (the void diameter) or R_d (the domain length) depending on the direction along which the perturbation is propagating. To take this into account we define the order parameter correlation length $\xi_g^{(phase)}$ of a confined system as

$$\xi_g^{(phase)} \sim \sqrt{\frac{1}{(R_g)^2} + \frac{1}{(\xi^{(phase)})^2}}. \tag{5.15}$$

In the limits $\xi^{(phase)}/R_g << 1$ and $\xi^{(phase)} = R_g >> 1$ this ansatz yields $\xi_g^{(phase)} \sim \xi^{(phase)}$ and $\xi_g^{(phase)} \sim R_g$, respectively. Here $\xi^{(phase)}$ stands for the nematic ($\xi^{(n)}$) and smectic ($\xi^{(s)}$) order parameter correlation length. We further assume that perturbed hydrodynamic fields typically change on the scale given by R_g.

Therefore in CPG samples we typically expect the following magnitudes of elastic distortions $|\nabla S| \sim \frac{\Delta S}{\xi_g^{(n)}}, |\nabla \eta| \sim \frac{\Delta \eta}{\xi_g^{(s)}}, |\nabla \vec{n}| \sim \frac{\varepsilon_n}{R_g}, |\nabla \delta\phi| \sim \frac{\varepsilon_\phi}{R_g}$. Here $\Delta S \sim |S_i - S| \sim \varepsilon_s S$, $\Delta\eta \sim |\eta_i - \eta| \sim \varepsilon_\eta \eta$, and ε_n, ε_ϕ measure the magnitude of changes in the hydrodynamic fields on the distance R_g. Typically, $1 > \varepsilon_s \sim \varepsilon_\eta \sim \varepsilon_n \sim \varepsilon_\phi > 0$.

The quantity $\delta\phi = \phi - \vec{n}\cdot\vec{r}\, q_o$ measures deviations of the phase ϕ from its bulk equilibrium value. We have assumed that the main distortions in order parameter fields take place at the LC-CPG interface and that this contribution overwhelms the contribution arising from topological defects.

For mathematical convenience we introduce the scaled order parameters $q_n = S/S_0$, $q_s = \eta/\eta_0$, where $S_0 = S_b(T = T_{IN})$ and $\eta_0 = \eta_b(T = 0)$. Taking all this into account (for details see Ref.[19]) we end up with the dimensionless free energy density $\Omega = \frac{2F}{\pi R^2 R_d a_0 (T_{IN} - T_*) S_0^2}$, expressed as

$$\Omega = t_n q_n^2 - 2q_n^3 + q_n^4 - \sigma_n q_n + A^2 \left(t_s q_s^2 + \frac{q_s^4}{2} - \sigma_s q_s \right). \tag{5.16}$$

Here $A = \xi_{\max}^{(n)}/(\xi_{\min}^{(s)} \lambda_{\min} q_0)$, $\xi_{\max}^{(n)} \equiv \xi^{(n)}(T = T_{IN})$, $\xi_{\min}^{(s)} \equiv \xi_s(T = 0)$, and $\lambda_{\min} = \sqrt{LS_0^2/(2C\eta_0^2 q_0^2)}$ is the smectic penetration length at $T = 0$. For typical LCs one finds $\xi_{\max}^{(n)} \gtrsim 10nm$, $\lambda_{\min} \sim \xi_{\min}^{(s)} \lesssim 1nm$. The quantities t_n and t_s stand for the effective nematic and smectic dimensionless temperature and σ_n and σ_s for the effective nematic and smectic ordering field:

$$t_n = \frac{T - T_*}{T_{IN} - T_*} - \frac{2\left(\xi_{\max}^{(n)}\right)^2}{R d_e^{(n)}} + \tag{5.17}$$

$$+ \left(\frac{\varepsilon_s \xi_{\max}^{(n)}}{\xi_g^{(n)}} \right)^2 \left(1 - \left(1 - \frac{\xi_g^{(n)}}{R} \right)^2 \right) + \left(\frac{\varepsilon_n \xi_{\max}^{(n)}}{R_g} \right)^2, \tag{5.18}$$

$$t_s = \frac{T - T_{NA}}{T_{NA}} - \frac{2\left(\xi_{\min}^{(s)}\right)^2}{R d_e^{(s)}} - d_{cp} q_n + \tag{5.19}$$

$$+ \left(\frac{\varepsilon_\eta \xi_{\min}^{(s)}}{\xi_c^{(s)}} \right)^2 \left(1 - \left(1 - \frac{\xi_g^{(s)}}{R} \right)^2 \right) + \left(\frac{\varepsilon_\phi \xi_{\min}^{(s)}}{R_g} \right)^2, \tag{5.20}$$

$$\sigma_n = \frac{2\left(\xi_{\max}^{(n)}\right)^2}{R d_e^{(n)}}, \tag{5.21}$$

$$\sigma_s = \frac{2\left(\xi_{\min}^{(s)}\right)^2}{R d_e^{(s)}}. \tag{5.22}$$

The quantities $d_e^{(n)} = \frac{LS_0}{W_{sam}^{(n)}}$, $d_e^{(s)} = \frac{C\eta_0}{W_{sam}^{(s)}}$ are the LC extrapolation lengths, and $d_{cp} = 2D\eta_0^2 / (a_0(T_{IN} - T_*)S_0)$ is the dimensionless coupling constant between the smectic and nematic order parameter.

The phase behavior of a system described in terms of Ω is simple and already studied in detail if R_d is not treated as a variational parameter [23]. But the obtained estimates work rather well according to the recent calculation [24], in which R_d is allowed to vary. In the following we first discuss the *I-N* and afterwards the *N-SmA* phase transition behavior for the case, where R_d plays the role of the control parameter.

For $\sigma_n < \sigma_c \equiv 0.5$ the isotropic (i.e., paranematic for $\sigma_n > 0$) – nematic phase transition takes place when the condition $t_n = 1 + \sigma_n$ is realized. From this condition the expression for the phase temperature shift $\Delta T_{IN} = T_{IN} - T_{IN}(R)$ is obtained:

$$\frac{\Delta T_{IN}}{T_{IN} - T_*} = \left(\frac{\varepsilon_s \xi_{\max}^{(n)}}{\xi_g^{(n)}}\right)^2 \left(1 - \left(1 - \frac{\xi_g^{(n)}}{R}\right)^2\right) + \left(\frac{\xi_{\max}^{(n)}}{R_g}\right)^2 \varepsilon_n^2 - \frac{2\left(\xi_{\max}^{(n)}\right)^2}{R d_e^{(n)}}. \tag{5.23}$$

For $\sigma_n > \sigma_c$ the paranematic-nematic transition becomes gradual.

The character of the *N-SmA* transition strongly depends on σ_s and d_{cp}. We believe that in our samples the coupling constant d_{cp} is weak enough so that the bulk *N-SmA* transition is continuous. It is believed [25] that the disorder further decreases the value of d_{cp}. Consequently we limit for the sake of simplicity to the case $d_{cp} = 0$. In this case, for $\sigma_s = 0$, the *N-SmA* transition remains continuous at $t_s = 0$. From this condition the expression for the phase temperature shift $\Delta T_{NA} = T_{NA} - T_{NA}(R)$ is obtained:

$$\frac{\Delta T_{NA}}{T_{NA}} = \left(\frac{\varepsilon_\eta \xi_{\min}^{(s)}}{\xi_g^{(s)}}\right)^2 \left(1 - \left(1 - \frac{\xi_g^{(s)}}{R}\right)^2\right) + \left(\frac{\xi_{\min}^{(s)}}{R_g}\right)^2 \varepsilon_\phi^2 - \frac{2\left(\xi_{\min}^{(s)}\right)^2}{R d_e^{(s)}}. \tag{5.24}$$

For $\sigma_s > 0$ the N-SmA transition becomes gradual.

5.4. Phase behavior

We study the phase behavior of 8CB as a function of the characteristic void size *R*, anchoring conditions and temperature. In Figs. 5.2 and 5.3 we show the temperature dependence of the specific heat for non-treated (Fig. 5.2) and silane-treated (Fig. 5.3) samples. The main phase transition characteristics are summarized in Table 5.1.

Table 5.1. Phase transition temperature shifts for 8CB in controlled-pore glasses of various pore diameters 2R. Also shown are width of the Nematic phase ΔT_N and enthalpy changes of the IN and NA phase transitions. Labels "N" and "T" in the first column denote non-treated and silane-treated samples, respectively.

$2R$ (nm)	ΔT_{IN} (K)	ΔT_{NA} (K)	ΔT_N (K)	ΔH_{IN} (J/g)	δH_{IN} (J/g)	L_{IN} (J/g)	ΔH_{NA} (J/g)
8CB bulk	0.00	0.00	6.96	7.97±0.1	5.77±0.1	2.20±0.05	0.80±0.03
395.0 N	1.08	1.00	6.83	7.80±0.1	5.85±0.1	1.95±0.05	0.70±0.03
127.3 N	1.80	2.25	7.36	7.77±0.1	6.09±0.1	1.68±0.05	0.63±0.03
72.9 N	2.03	2.60	7.48	7.57±0.1	6.17±0.1	1.40±0.05	0.43±0.03
23.7 N	2.55	3.76	8.12	7.38±0.2	6.22±0.2	1.16±0.1	0.12±0.02
395.0 T	0.34	0.43	7.00	7.66±0.1	5.85±0.1	1.81±0.05	0.74±0.03
127.3 T	0.52	0.64	7.03	7.68±0.1	6.43±0.1	1.25±0.05	0.52±0.03
60.0 T	0.44	0.16	6.63	7.50±0.1	6.59±0.1	0.91±0.05	0.20±0.02
23.7 T	1.88	2.80	7.83	7.19±0.2	6.53±0.2	0.66±0.1	0.11±0.02

The phase behavior across the *I-N* phase transition in depicted in the upper part of Figs. 5.2 and 5.3. With decreasing R the phase transition region broadens and the phase transition temperature shift ΔT_{IN} progressively increases. According to our modeling the wetting at the void-LC interface is dominant in $\Delta T_{IN}(R)$. To show that we compare the temperature shift $\Delta T_{IN}^{(hyd)}(R) = (T_{IN} - T_*)\left(\frac{\xi_{\max}^{(n)}}{R_g}\right)^2 \varepsilon_n^2$ due to the elastic deformations in the director field and $\Delta T_{IN}^{(op)}(R) \sim (T_{IN} - T_*)\ \frac{2\left(\xi_{\max}^{(n)}\right)^2}{R\xi_g^{(n)}}\varepsilon_s^2$ due to deformations in the order parameter field. Here the superscripts $^{(hyd)}$ and $^{(op)}$ denote hydrodynamic and order parameter field distortions, respectively. Setting $\varepsilon_n \sim \varepsilon_s \sim 1$, $\xi_{\max}^{(n)} \sim \xi_g^{(n)} \sim 15$ nm, and $R_g \geq R$ we obtain $\Delta T_{IN}^{(hyd)}(15) \leq 1$ K, $\Delta T_{IN}^{(hyd)}(150) \leq 0.01$ K; $\Delta T_{IN}^{(op)}(15) \sim 2$ K, $\Delta T_{IN}^{(op)}(150) \sim 0.2$ K, where we have expressed R in nm. Here we have estimated the temperature shifts in the regime covered by our measurements. We further note that experiments reveal monotonic $\Delta T_{IN}(R)$ dependence. Only the temperature shifts due to the order parameter variations at the LC-void interface are close to the measured values of $\Delta T_{IN}(R)$ in the whole regime studied.

The same holds true for the *N-SmA* phase transition. The $\Delta T_{IN} = \Delta T_{IN}(R)$ and $\Delta T_{NA} = \Delta T_{NA}(R)$ dependencies show remarkable similarity. As in the *I-N* case we compare the temperature variations due to the elastic deformations in the phase field $\Delta T_{NA}^{(hyd)}(R) = T_{NA}\left(\frac{\xi_{\min}^{(s)}}{R_g}\right)^2 \varepsilon_\phi^2$ and due to deformations in the smectic order parameter field $\Delta T_{NA}^{(op)}(R) \sim T_{NA}\left(\frac{\varepsilon_\eta \xi_{\min}^{(s)}}{\xi_g^{(s)}}\right)^2 \left(1 - \left(1 - \frac{\xi_g^{(s)}}{R}\right)^2\right)$.

Setting $\varepsilon_\eta \sim \varepsilon_\phi \sim 1$, $\xi_{\min}^{(s)} \sim 1$ nm, $\xi_g^{(s)} \sim 15$ nm, and $R_g \geq R$ and $R_g \sim R$ we obtain $\Delta T_{NA}^{(hyd)}(15) \leq 1.3$, $\Delta T_{NA}^{(hyd)}(150) \leq 0.01$; $\Delta T_{NA}^{(op)}(15) \sim 1.4$, $\Delta T_{NA}^{(op)}(150) \sim 0.3$.

It is evident that the surface interaction contributions, that are directly proportional to $W_{sam}^{(phase)}$, play secondary role in $\Delta T_{IN}(R)$ and $\Delta T_{NA}(R)$. The local ordering wetting tendencies tend to increase the phase transition temperatures of both phases what is not observed. However the surface fields play important role in determining the character of phase transition. According to our model the *I-N* phase transition is expected to become gradual for $\sigma_n > 0.5$ and the *N-SmA* one for $\sigma_s > 0$, where $\sigma_j \propto 1/R$. Recent NMR measurements [26] support these predictions. They show that the *I-N* transition becomes gradual for $R < 20$ nm. We further note that stronger surface induced pretransitional phenomena (see Figs. 5.2 and 5.3) in silanized-samples suggests that $W_{sil}^{(phase)} > W_{non}^{(phase)}$.

In addition to surface wetting features the specific heat temperature dependence also reveals influence of randomness and finite size effects. To demonstrate that we focus on the N-SmA phase transition which remains sharp enough also in CPG confinements studied. Consequently we can perform critical exponent analysis. According to it the excessive heat capacity peak $\Delta C_p^{(\max)}$ at $T_{NA}(R)$ scales as

$$\Delta C_p^{(\max)} = A^{\pm} |r|^{-\alpha_{eff}} \left(1 + D^{\pm} |r|^{0.5}\right) + B. \tag{5.25}$$

The coefficients $A^{\pm}$, $D^{\pm}$, and B represent the usual amplitude, correction- to scaling amplitude and critical background, respectively. $\alpha_{eff}(R)$ is the effective critical exponent and $r = (T - T_{NA}(R))/T_{NA}(R)$ is the reduced temperature. The + (-) sign corresponds to coefficients above (below) the transition temperature. Nonlinear least-square fits were performed for a maximum reduced temperature $|r_{\max}|$ with range shrinking by expanding $|r_{\min}|$ for a specific factor (2 – 5 in CPG samples, 2 – 20 in pure 8CB) in order to test the stability of the fit parameters. We found out that although rather favorable χ_ν^2 could be obtained, the fits to data for the pore diameters below 100 nm suffer from considerable rounding effects and were not stable against range shrinking. Consequently the results obtained for $2R < 100$ nm are only tentative.

In the upper part of Fig. 5.4 we show the results of such analysis. One sees that $\alpha_{eff}(R)$ decreases with decreasing R, particularly in non-treated samples. Similar behavior is observed also in LC-aerosil mixtures [25], suggesting the universal response of LCs to random environments. A possible explanation is that with decreasing R the degree of disorder increases. In pure 8CB the value of $\alpha \sim 0.27$ is close to the tricritical one. At the tricritical point, determined by

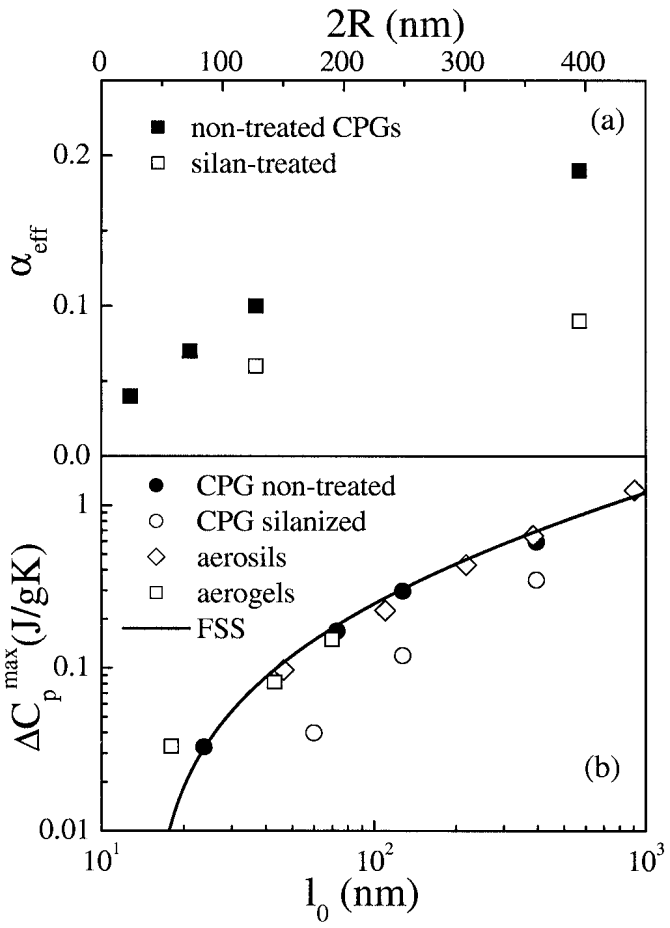

Figure 5.4. (a) The effective critical α_{eff} as a function of the characteristic cavity radius. (b) The peak value of the $\Delta C_p^{(max)}$ at the N-SmA transition as a function of the mean-open length l_0. The full line is calculated using the finite size scaling (FSS) approach.

the critical value of the coupling constant $D \equiv D_c$, the *N-SmA* transition crosses from continuous (for $D < D_c$) to discontinuous (for $D > D_c$) character. With decreasing R the value of α decreases, approaching the 3D-XY value $\alpha = -0.013$ [25]. In this limit the smectic and nematic order parameter are completely decoupled.

In addition the specific heat peak $\Delta C_p^{(max)}(R)$ dependence reveals finite size effects in non-treated samples. For this purpose we assume that at $T_{NA}(R)$ the divergence of $\Delta C_p^{(max)}$ is limited by finite size effects. Consequently we equal the order parameter correlation length ξ at the transition with the characteristic confinement length l_0 of the system and consider that $\xi \sim \xi_0/|r|^{\nu}$. Here $\xi_0 \sim 0.9$ nm is the bare correlation length and ν the corresponding critical coefficient. For CPG matrices we assume $l_0 = 2R$ and set $|r| = (\xi_0/l_0)^{1/\nu}$ in Eq.(5.25). By putting the bulk values for critical coefficients (i.e., $\alpha_{eff} = \alpha_b \sim 0.27$, $\nu = \nu_b \sim 0.5$) we reproduce the scaling prediction in non-treated samples as shown in Fig. 5.4, bottom part. In case of silane-treated samples the finite scaling is not

obeyed. Here the $\Delta C_p^{(\max)}(R)$ dependence is dominated by surface interaction effects. This is due to stronger interface coupling in silanized samples.

Note that finite scaling is obeyed also in aerogel matrices [4] and LC-aerosil mixtures [25], again proving the universal behavior. In Fig. 5.4 we demonstrate this universality, where l_0 in (i) aerogel-LC and (ii) aerosil-LC mixtures corresponds to (i) the mean void pore chord of the aerogel matrix and (ii) the average separation between aerosil units.

5.5. Conclusions

We studied the influence of CPG confinement on the *I-N* and *N-SmA* temperature driven phase transition using high resolution calorimetry. The CPG matrices were either treated with silane or non-treated. Consequently, the homeotropic or isotropic tangential anchoring was imposed to LC molecules, respectively. We analyzed the phase behavior using a simple Landau-de Gennes type approach. In it the phase and configuration within it were described with the relevant order parameter and hydrodynamic field, respectively. The critical behavior of the *N-SmA* phase transition was further analyzed using the critical exponent analysis.

In all samples the *I-N* transition remained discontinuous. There are however indications that the transition becomes gradual for $R < 10$ nm as also suggested by NMR studies [26]. The *N-SmA* transitions are continuous or gradual, but with emphasized continuous-type phase transition features. Both *I-N* and *N-SmA* phase transition temperature shifts display qualitative similarities as a function of R and they are mainly controlled by LC-void wetting feature. In non-treated samples, the specific heat amplitude at the *N-SmA* transition perfectly obeys the finite size scaling prediction for $R > 12$ nm. This scaling has also been observed in 8CB-aerosil mixtures [25]. In silane-treated samples the finite size effects are screened by surface wetting interactions. The $\alpha(R)$ dependence in all samples further suggests that with decreasing value of R the influence of disorder increases. We have shown that the critical exponent α exhibits a crossover from the nearly tricritical behavior in the bulk sample towards 3D-XY value with decreasing R. This feature have been also observed in LC-aerogel [27] and LC-aerosil [25] samples.

Bibliography

1. *Liquid Crystals in Complex Geometries formed by polymer and porous networks*, eds. G.P. Crawford, S. Zumer (Taylor and Francis, London, 1996).
2. P.G. de Gennes, Science **265**, 495 (1992).
3. M.D. Dadmun and M. Muthukumar, J. Chem. Phys. **98**, 4850 (1993).
4. Z. Kutnjak, S. Kralj, G. Lahajnar, and S. Zumer, Phys. Rev. E **68**, 021705 (2003); ibid. **70**, 051703 (2004).

5. G.S. Iannacchione, G.P. Crawford, S. Zumer, J.W. Doane, and D. Finotello, Phys. Rev. Lett. **71**, 2595 (1993).
6. F.M. Aliev and M.N. Breganov, Zh. Eksp. Teor. Fiz. **95**, 122 (1989) [Sov. Phys. JETP **68**, 70 (1989)]
7. L. Wu, B. Zhou, C.W. Garland, T. Bellini, and D.W. Schaefer, Phys. Rev. E **51**, 2157 (1995), and references therein.
8. Z. Kutnjak and C.W. Garland, Phys. Rev. E **55**, 488 (1997).
9. N.A. Clark *et al.*, Phys. Rev. Lett. **71**, 3505 (1993).
10. A. Mertelj and M. Copic, Phys. Rev. E **55**, 504 (1997).
11. H. Zeng, B. Zalar, G.S. Iannacchione, and D. Finotello, Phys. Rev. E **60**, 5607 (1999).
12. G.P. Sinha and F.M. Aliev, Phys. Rev. E **58**, 2001 (1998).
13. G. Schwalb and F.W. Deeg. Phys. Rev. Lett. **74**, 1383 (1995).
14. Y. Imry and S. Ma, Phys. Rev. Lett. **35**, 1399 (1975).
15. D. Feldman, Phys. Rev. Lett. **84**, 4886 (2000).
16. M.A. Anisimov *et al*., Phys. Rev. A **41**, 6749 (1990), and references therein.
17. H. Yao and C.W. Garland, Rev. Sci. Instrum. **69**, 172 (1998).
18. P. G. de Gennes and J. Prost, *The Physics of Liquid Crystals* (Oxford University Press, Oxford, 1993).
19. S. Kralj, V. Popa-Nita, and M. Svetec, Random anisotropy liquid crystal model. Contribution in this book.
20. L. Radzihovsky and J. Toner, Phys. Rev. B **60**, 206 (99).
21. M. Cagnon and G. Durand, Phys. Rev. Lett. **70**, 2742 (1993).
22. S. Kralj and T.J. Sluckin, Phys. Rev. E. **50**, 2940 (1994).
23. D.J. Cleaver, S. Kralj, T.J. Sluckin, and M.P. Allen, in *Liquid Crystals in Complex Geometries formed by polymer and porous networks*, eds. G.P. Crawford, S. Zumer, Taylor and Francis, London, (1996), 467.
24. S. Kralj and V. Popa-Nita, Eur. Phys. J E **14**, 115 (2004).
25. G.S. Iannacchione, S. Park, C.W. Garland, R.B. Birgeneau, and R.L. Leheny, Phys. Rev. E **67**, 011709 (2003).
26. S. Kralj, A. Zidansek, G. Lahajnar, S. Zumer, R. Blinc, Phys. Rev. E **57**, 3021 (1998).
27. G.S. Iannacchione, C.W. Garland, J.T. Mang, and T.P. Rieker, Phys. Rev. E **58**, 5966 (1998).